Slab dehydration in the Earth's mantle transition zone

Guillaume Richard *, David Bercovici, Shun-Ichiro Karato

Department of Geology and Geophysics, Yale University, United States

Abstract

Because of the high water solubility in wadsleyite and ringwoodite, the mantle transition zone is possibly a large water reservoir. The potentially high water content of the Earth's mantle transition zone is a key element of several global mantle dynamic models. Nevertheless, to keep the transition zone relatively wet, the tendency for convection to distribute water over the entire mantle has to be offset by other mechanisms. One such mechanism could be linked to the dehydration of the slab. Studies of slab dehydration mainly focus on hydrous minerals phase diagrams that provide the depth of water exsolution. In this study, we investigate the water diffusion process that occurs prior to such exsolution. The diffusion process is controlled by both chemical gradients and thermal gradients via the temperature dependence of water solubility. We have addressed how this diffusion phenomenon influences slab water transport into the transition zone by developing a theoretical model of coupled thermal and chemical diffusion in a flat lying slab stalled in the transition zone.

Model solutions demonstrate that even if intrinsic water solubility is decreasing with increasing temperature (which normally would act to impede a chemical diffusion from the slab), the water concentration profile adjusts to reduce the adverse effects of temperature-dependent solubility. The self-adjustment entails the concentration of water reaching a local maximum below the top edge of the stagnant slab; under specific conditions, this concentration maximum can reach the solubility limit and thus exsolve fluid (i.e. create of hydrous melt or aqueous silicate fluid). Consequently, model water flux computations are relatively independent of solubility variation and indicate that much of the water flux introduced by relatively well hydrated slabs is taken up into the transition zone by diffusion.

© 2006 Published by Elsevier B.V.

Keywords: Water; Double diffusion; Stagnant slab; Transition zone; Water solubility

1. Introduction

Water plays various important roles in controlling the dynamics and evolution of the Earth's interior. Two areas in the Earth's mantle are able to store large amounts of water, i.e., the oceanic crust and lithosphere and the transition zone (between 410 km and 660 km depths). The oceanic crust and shallow lithosphere undergo lengthy traverses along the bottom of the oceans and are thus well hydrated. Subduction transports some of this water into the mantle, although how much water is transported this way remains unclear [1–3]. However, even if a large part of the subducted water was released back to the hydrosphere through arc volcanism, in cold slabs a significant amount (∼40% of its initial water

* Corresponding author.
E-mail address: guillaume.richard@yale.edu (G. Richard).

content) is released by the breakdown of sediments, crust, and serpentinized mantle at high pressure and temperature [2] is likely stored in various dense hydrous magnesium–silicate phases (DHMS) that can be carried to depths of 450 km [3–5]. At depths between 410 and 660 km, in the transition zone, the water solubility is very high and the water can be stored in ringwoodite (up to 2.4 wt.%) or in wadsleyite (up to 2.7 wt.%) [6]. The amount of water that slabs can carry down to the transition zone storage area depends on the transit time of slabs across the transition zone. In particular, tomographic imaging depicts many slabs deflected horizontally and lingering in the transition zone [7]. One unresolved question concerns the way water, carried by a subducting slab, behaves when it enters and dwells in this high solubility area. Global models like the transition zone water-filter model [8] and electrical conductivity data [9] suggest that the transition zone water reservoir is slightly hydrated (of order of 0.1 wt.% or less than 10% of its capacity). Convective mixing on the mantle tends to prevent the transition zone from soaking up water by simple diffusion from the lower and upper mantles, where water solubility is lower [10]. Therefore, other processes are required to bring water into this reservoir. Previous studies have described two processes providing water: one "from the bottom" and one "from the top". Upward percolation of water expelled from slabs entering the low-solubility lower mantle at 660 km depth is likely to be one way to hydrate the transition zone [8,11]. At the transition zone upper boundary (410 km depth), the possible melt layer of the water-filter model [8] caused by dehydration of supersaturated upwelling mantle provides a trap and source of water which would be entrained back into the transition zone by slabs [8,12].

Another way to hydrate the transition zone is from dehydration of slabs stagnating in the transition zone. This dehydration is controlled by the stability of dense hydrous magnesium silicates (DHMS) [13]. Given the phase diagrams of these DHMS under the pressures of interest, fluid exsolution can be located at certain depths and temperature. However, water can also leave the slab without invoking exsolution of fluids. Because water concentration in the slab is higher than in the surrounding mantle, diffusion will take place. In this case, one important effect influencing water transport is the temperature-dependence of water solubility in the system $MgO–SiO_2–H_2O$. Under high temperature ($T > 200$ °C) and pressure (i.e. transition zone) conditions, experiments done under wet conditions indicate that the transition minerals wadsleyite and ringwoodite always coexist with a fluid (certainly close to a hydrous

melt) that contains abundant dissolved oxides, and the presence of such fluids is likely to influence solubility measurements [14]. Because of these fluids and of the temperature dependence of water fugacity [15], the measured water storage capacity decreases with increasing temperature in wadsleyite [14] and in ringwoodite [16]. However, as shown below (see Appendix B.2), water fugacity does not play any role in the diffusion process and thus the effect of fugacity on the temperature dependence of solubility must be removed before evaluating the chemical potential of water in transition zone minerals. As detailed below (cf. Section 2.1), the intrinsic chemical potential mainly controls the temperature dependence of water solubility and thus influences the water diffusion process, and affects both the water concentration profile in this region as well as the flux of water out of the slab. Our goal is to understand how the temperature dependence of water solubility influences slab water transport into the transition zone. To do so, we have developed and explored a theoretical model to describe the basic physical process of coupled chemical and heat transport at the slab-mantle interface.

2. Model description

Our theoretical model describes transport of water out of and heat into a slab temporarily floating in the transition zone (Fig. 1). The two transport processes are coupled by the temperature dependence of water solubility in transition zone minerals.

2.1. Coupling of the heat and water fluxes

One can employ the formalism of linear nonequilibrium thermodynamics (see [17]) to define the fluxes and conjugate or thermodynamics forces of our system (see Appendix B.1 for details). According to the second law of thermodynamics, the rate of entropy production is
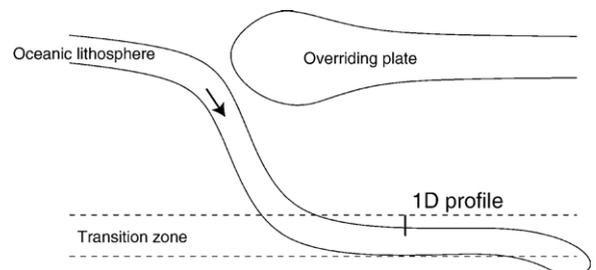
Fig. 1. The dehydration of a stagnant slab in the mantle transition zone The essence of the model hypothesis: The diffusion of water out of the slab and the diffusion of heat into the slab occur simultaneously and are coupled by the temperature dependence of the water solubility.

positive–definite and in general the heat flux $\mathbf{J}_T$ (J m^{-2} s^{-1}) and the chemical (water) flux $\mathbf{J}_W$ (mol m^{-2} s^{-1}) are coupled such that:

$$\begin{cases} \mathbf{J}_T = L_{11} \nabla \dfrac{1}{T} - L_{12} \nabla \dfrac{\mu}{T} \\ \mathbf{J}_W = L_{12} \nabla \dfrac{1}{T} - L_{22} \nabla \dfrac{\mu}{T} \end{cases} \qquad (1)$$

where L_{ij} (i, $j=1$, 2) are called phenomenological coefficients (or elements in a positive–definite matrix), μ is the chemical potential of water and T is the temperature. The Onsager reciprocal theorem tells us that $L_{12} = L_{21}$ [18]. In our system, the heat diffusivity is much higher than the water diffusivity and it can be shown (see Appendix B.1) that chemical heat transport $L_{12}\nabla\frac{\mu}{T}$ is negligible compared to $L_{11}\nabla\frac{1}{T}$. Assuming that $\frac{L_{21}}{L_{22}}$ is a constant, $\mathbf{J}_W$ can also be recast to yield:

$$\begin{cases} \mathbf{J}_T = L_{11} \nabla \dfrac{1}{T} = -k \nabla T \\ \mathbf{J}_W = -R L_{22} \nabla \dfrac{\mu - \frac{L_{21}}{L_{22}}}{RT} \end{cases} \qquad (2)$$

where R is the gas constant and k the thermal conductivity. The chemical potential is given by $\mu = \mu^0 + RT\ln(a)$, where μ^0 is the standard-state chemical potential of dissolved water. Water concentration (–OH) is directly proportional to the concentration of magnesium vacancies V''_{Mg} that we assume to be ideally mixed [19], thus the activity a can be replaced by the water concentration C. Introducing the water solubility [6],

$$C^* = \frac{f_{H_2O}}{P_0 a_{MgO}} e^{-\frac{\mu^0 - \Delta\mu^0}{RT}} \qquad (3)$$

the chemical potential reads (see Appendix A):

$$\mu = \mu^0 + RT\ln(C) = \Delta\mu^0 + RT\ln\left(\frac{f_{H_2O}}{P_0 a_{MgO}}\frac{C}{C^*}\right) \qquad (4)$$

where $\frac{f_{H_2O}}{P_0}$ is the dimensionless water fugacity, $\Delta\mu^0$ is the standard-state chemical potential variation (see Table D.1 for definition) and a_{MgO} is the magnesium oxide activity.

Introduction of Eq. (4) into the expression for the flux $\mathbf{J}_W$ in Eq. (2) (see Appendix B.2 for a detailed derivation) leads to:

$$\mathbf{J}_W = -\alpha(-C\nabla\ln\overline{C}^* + \nabla C) = \mathbf{J}_W^* + \mathbf{J}_W^C \qquad (5)$$

where $\alpha = \dfrac{L_{22}R}{C}$ is the water diffusivity which we assume is constant, and $\overline{C}^*$ is the intrinsic (or effective) solubility defined as:

$$\overline{C}^* = \frac{P_0 a_{MgO}}{f_{H_2O}} e^{-\frac{\Delta\mu^0 - \frac{L_{21}}{L_{22}}}{RT}} C^* = e^{-\frac{\mu^0 - \frac{L_{21}}{L_{22}}}{RT}} = e^{-\frac{E}{RT}} \qquad (6)$$

where we introduce $E = \mu^0 - \dfrac{L_{21}}{L_{22}}$ hereafter referred as the 'intrinsic' chemical potential. At high pressure, the water

Table D.1
Used variables and parameters

Symbols	Names	Values	Units
κ	Thermal diffusivity	10^{-6}	m^2 s^{-1}
k	Thermal conductivity	3.3	Jm^{-1} s^{-1} K-1
α	Water diffusivity	$10^{-8} - 10^{-10}$	m^2 s^{-1}
C^*	Water solubility	$\frac{f_{H_2O}}{P_0 a_{MgO}} e^{-\frac{\mu^0 - \Delta\mu^0}{RT}}$	mol^{-1}
μ^0	Standard-state chemical potential of bonded water	$-100 - +100$	kJ mol^{-1}
$\frac{f_{H_2O}}{P_0}$	Dimensionless water fugacity	$10^9 - 10^{10}$	–
a_{MgO}	MgO chemical activity	0.5	–
μ_i^0	Standard-state chemicalppotential of element I	–	kJ mol^{-1}
Δ_μ^0	Standard-state chemical potential variation	$\mu_{H2O}^0 + \mu_{Mg}^0 - \mu_{MgO}^0$	kJ mol^{-1}
C	Water concentration	$\overline{C} - \frac{\delta C}{2}\Phi_{(\eta)}$	wt.%
$\overline{C}$	Average temperature on the studied profile	$0.5 - 2$	wt.%
δC	Concentration	$0.5 - 2$	wt.%
T	Temperature	$\overline{T} - \frac{\delta T}{2}\theta(\eta)$	°C
$\overline{T}$	Average temperature on the studied profile	$1300 - 1400$	°C
δT	Temperature range	$300 - 400$	°C
ρ	Mantle density	3300	kg m^3
C_P	Mantle thermal capacity at constant pressure	10^3	J. kg^{-1} K^{-1}
η	Similarity variable	$\frac{z}{2\sqrt{\kappa t}}$	–
$\Phi(\eta)$	Normalized water concentration	$-1 - +1$	–
$\theta(\eta)$	Normalized temperature	$-1 - +1$	–

fugacity decreases strongly with increasing temperature [15] and thus the temperature dependence of C^* and $\bar{C}^*$ can have opposite trends (see Appendix D).

The water flux can be seen as the combination of two fluxes: $\mathbf{J}_W^C = -\alpha \nabla C$, which depends on the concentration gradient as expected; and $\mathbf{J}_W^* = \alpha C \nabla \ln \bar{C}^*$, which depends on the intrinsic solubility gradient. If the water solubility were the same between the slab and the surrounding mantle, then the flux would be $\mathbf{J}_W = \mathbf{J}_W^C = -\alpha \nabla C$. Alternatively, if the concentration were constant, the flux would be driven by the solubility gradient. The actual water flux $\mathbf{J}_W$ will be reduced or enhanced compared to $\mathbf{J}_W^C$, depending on the sign of $\nabla \ln \bar{C}^*$. Because the intrinsic solubility $\bar{C}^*$ is temperature dependent the heat $\mathbf{J}_T$ and chemical fluxes $\mathbf{J}_W^*$ are coupled.

2.2. Diffusion equations and 1D similarity solution

In a Lagrangian coordinate system following the horizontal motion of the slab, diffusion of a quantity X is given by $\frac{dX}{dt} = -\nabla \cdot \mathbf{J}_X$. Thus, introducing the thermal diffusivity $\kappa = \frac{k}{\rho C p} = L_{11}/T^2$, which is assumed constant, to recast Eq. (5), our system can be described using the following set of equations (see Appendix B.2):

$$\begin{cases} \dfrac{dT}{dt} = \kappa \nabla^2 T \\ \dfrac{dC}{dt} = \nabla \left(\alpha \bar{C}^* \nabla \left(\dfrac{C}{\bar{C}^*} \right) \right) \end{cases} \tag{7}$$

In a one-dimensional system in which variation is only along the z-axis (where z is the distance from the slab-mantle interface), the system (7) permits similarity solutions for both the temperature and water concentration profiles. We write T the temperature profile as $T = \bar{T} + \frac{\delta T}{2} \theta(\eta)$, where $\bar{T}$ is the average temperature as well as the temperature at the slab mantle interface, δT the temperature step between slab and mantle and $\theta(\eta)$ is a function of the similarity variable $\eta = \frac{z}{2\sqrt{\kappa t}}$. Thus, the heat diffusion equation becomes

$$-2\eta \frac{d\theta}{d\eta} = \frac{d^2\theta}{d\eta^2} \tag{8}$$

which yields the well-known error function solution; with boundary condition that $T = \bar{T}$ at $z=0$, or $\theta = 0$ at $\eta = 0$, the solution to Eq. (8) is

$$\theta(\eta) = \mathrm{erf}(\eta) \tag{9}$$

Writing the water concentration $C = \bar{C} + \frac{\delta C}{2} \Phi(\eta)$, where $\bar{C}$ is the average concentration as well as the

concentration at the slab mantle interface and δC the concentration step, we can recast the water diffusion equation as:

$$\frac{\delta C}{2} \frac{d\Phi}{dt} = \alpha \frac{\partial}{\partial z} \left(\frac{\delta C}{2} \frac{\partial \Phi}{\partial z} - \frac{\bar{C} + \frac{\delta C}{2} \Phi}{\bar{C}^*} \frac{\partial \bar{C}^*}{\partial z} \right) \tag{10}$$

For the sake of simplicity, using a Taylor expansion around $\bar{T}$ we can rewrite the intrinsic solubility (6) as

$$\bar{C}^* = e^{-\frac{E}{RT}} = B e^{A\theta} \tag{11}$$

The parameters $A = \frac{E}{R\bar{T}} \frac{\delta T}{2\bar{T}}$ and $B = e^{-\frac{E}{R\bar{T}}}$ are not well constrained for transition-zone minerals, mainly because E, the intrinsic chemical potential of dissolved water, is unknown. The sign of E, controls the sense of variation of the intrinsic solubility with temperature: the intrinsic solubility increases with temperature when E is positive and decreases when E is negative. After substitution of Eq. (11) and the similarity variable η into Eq. (10) we obtain the ordinary differential equation for Φ:

$$\frac{d^2\Phi}{d\eta^2} + \left(\frac{2\kappa\eta}{\alpha} - A \frac{d\theta}{d\eta} \right) \frac{d\Phi}{d\eta} - A \frac{d^2\theta}{d\eta^2} \Phi - 2A \frac{\bar{C}}{\delta C} \frac{d^2\theta}{d\eta^2} = 0 \tag{12}$$

The far-field boundary conditions are that $\Phi \to \mp 1$ as $\eta \to \pm\infty$. To solve (12), we employ a 1D second-order finite-differences implicit scheme. We use 10,000 grid points in the domain $-10 \le \eta \le 10$ that is large compared to the intrinsic diffusive length scales (i.e. $\eta = 10$ is effectively equivalent to $\eta \to \infty$) and prevents boundary effects.

3. Results

We seek to quantify the effects of the double diffusion process on water transport from a slab into the transition zone. Uncertainties in some of the controlling parameters, such as the intrinsic chemical potential E and water diffusivity α, are large. Unfortunately, high-pressure experiments [14,16] on transition zone water solubility have included an aqueous phase or melting of the transition zone mineral and are thus not relevant to describe a solid state diffusion process. Consequently, we have explored a large range of values to investigate their influences, especially $E = \mu^0 - \frac{L_{21}}{L_{22}}$, on the water concentration profile and water flux away from the slab.

3.1. Water concentration profiles and diffusive coupling

Eq. (12) shows that the coupling effect is related to the ratio between $\frac{\kappa}{\alpha}$ and A. If $\frac{\kappa}{\alpha}$ is relatively large $\left(\frac{\kappa}{\alpha} \gg A\right)$, then the three temperature dependent terms (proportional to A) can be neglected leaving the water concentration largely independent of temperature.

For the case where $\frac{\kappa}{\alpha} \sim A$, E becomes an important parameter. Its sign controls the direction of the solubility driven water flux $\mathbf{J}_W^*$ (see Eq. (5)) and its magnitude dictates the strength of this flux. In particular, if the sign of E is negative, the water flux driven by chemical and solubility gradients are opposite. The competition between these two fluxes induces a local increase of the water concentration at the edge of the slab. Under specific initial conditions, this effect could yield water concentrations up to the solubility limit of the mantle mineral, which can then induce water exsolution and/or melting.

3.1.1. Water accumulation

Under high pressure, in transition zone minerals, water fugacity decreases with increasing temperature [15]. Experimental studies [14,16] suggest that water storage capacity decreases with increasing temperature, but because of the presence of fluid (aqueous solution or melt) in these experiments, obtaining the value of E is not straight forward. Uncertainties on water fugacity, phenomenological coefficients, chemical potential and linked to fluid presence have to be summed up and become large. Thus we make no assumptions on the trend of this temperature dependence but instead explore the full plausible range of E ($E \in [-100, +100]$kJ mol^{-1}).

We have run several simulations to understand how E influences the water concentration profile. If the intrinsic water solubility increases with temperature ($E > 0$), the two water fluxes ($\mathbf{J}_W^*$, $\mathbf{J}_W^C$) are in the same direction. This effect enhances the diffusion of water out of the cold region to the warmer mantle and the shape of the concentration profile is close to an error-function shape (see Fig. 4 and Section 3.2 below). In contrast, in negative E cases (wherein intrinsic solubility decreases with increasing temperature), the resulting water concentration profiles (Fig. 2) depict a local maximum within the slab below the mantle-slab interface. On either side of this chemical flux convergence zone, the two forces that drive the water flux are opposite. On the one hand, water tends to diffuse, as usual, from a high concentration region (wet slab) to low concentration one (dry mantle), but on the other hand it tends to diffuse away from low solubility area (warm mantle) towards high solubility area (cold
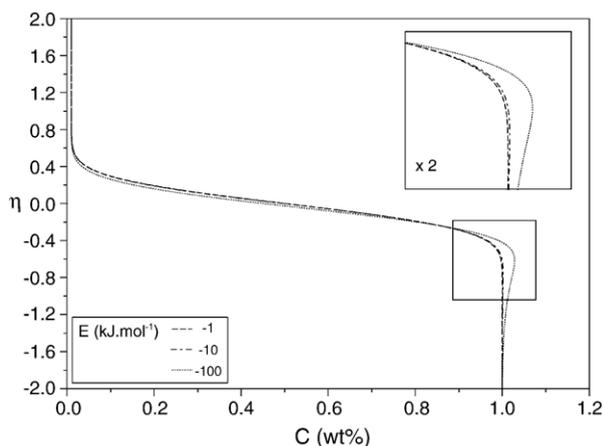
Fig. 2. Temperature effect on water diffusion in the transition zone with $\mu^0 < 0$. Water concentration profile of a 1 wt.% hydrated slab diffusing in a dry surrounding mantle (0.01 wt.%). When $E < 0$ the intrinsic water solubility decreases with increasing temperature and the double diffusion effect induces the creation of local maximas within the water concentration. This feature also affects the water flux away from the slab (see Section 3.2). The three displayed profiles correspond to $E = -1, -10, -100$ kJ mol^{-1} to represent water solubilities that are is weakly to strongly temperature dependent. To emphasize the local maxima, we have set a high water diffusivity ($\alpha = 10^{-7} m^2 s^{-1}$, $\frac{\kappa}{\alpha} = 10$). The y-axis is the similarity variable $\eta = \frac{z}{2\sqrt{\kappa t}}$, where κ the thermal diffusivity is about 10^{-6} m^2 .s^{-1}.

slab). It is evident in Fig. 2 that the 'concentration maximum' is more important when $|E|$ is large.

3.1.2. Water supersaturation

A consequence of the formation of a local maximum of water concentration, if it is large enough, is the crossing of the solubility limit and the formation of a super-saturated region. To illustrate the effect of double diffusion (coupling between thermal and water diffusion) on water supersaturation, we present a case where the true solubility C^* increases with increasing temperature. Here, supersaturation is more difficult to reach than in a case where the true solubility decreases with increasing temperature and can thus be considered a limiting case. Recall that the true C^* (Eq. (3)) and intrinsic solubility C^* (Eq. (6)) can have opposite temperature dependences (see Appendix D).

In the calculations displayed in Fig. 3, we have considered a slightly under-saturated slab with an initial water concentration C_{slab}^0 of 2.4 wt.% lingering in a mantle containing 0.01 wt.% of water. The slab and mantle are composed of a 10 mineral whose water solubility is 2.41 wt.% at 1100 °C and 3 wt.% at 1500 °C. If E is strongly negative ($E < -200$ kJ mol^{-1}) then the local maximum in water concentration can reach the solubility limit and hence supersaturation.
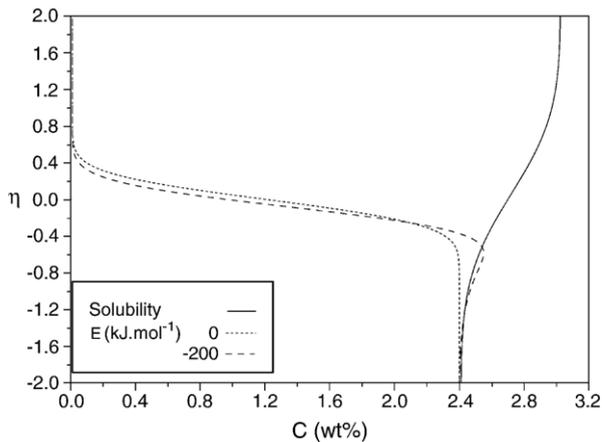
Fig. 3. Double diffusion effect and liquid release Water concentration profile as a function of $\eta = \frac{z}{2\sqrt{\kappa t}}$ for a large negative chemical potential $E = -200 \text{ kJ mol}^{-1}$, a high water diffusivity $\alpha = 10^{-7} \text{ m}^2 \text{ s}^{-1}$ and an initial water concentration in the slab close to saturation ($C_{\text{slab}}^0 = 2.4$ wt.%). The concentration profile (long dashed line) displays a local maxima below the edge of the slab that is larger than the solubility limit (solid line). $\kappa = 10^{-6} \text{ m}^2 \text{ s}^{-1}$. See text for details.

Therefore if the slab entering the transition zone is close to saturation, the water concentration (dashed line) intersects the true solubility limit (solid line). In this case, water is released from the minerals and produces aqueous fluid or hydrous melt. The likeliness of this fluid release depends on the amount of water carried by the slab down to the transition zone and by the water concentration of the surrounding mantle at this depth (410 km). If the initial slab water concentration is high enough, the peak water concentration can reach the solubility limit and thus induce water exsolution or melting at the edge of the slab even if the true solubility of water is increasing with temperature. The flux of water from the slab would be strongly enhanced by such a mechanism. It is worth noting that this mechanism of water exsolution is very similar to the exsolution of water from hydrous minerals that are unstable. In our case, exsolution occurs because the intrinsic water solubility decreases while the slab temperature increases with time. In the case of unstable hydrous minerals, exsolution occurs because the mineral disappears when the temperature increases, thus expelling water.

3.2. Flux of water away from the slab

A subducted slab is likely to transport a relatively large amount of water into the transition zone. Laboratory experiments [3,5] and numerical models [2] argue that the top (5–10 km thick) of a cold subducting peridotitic lithosphere is able to carry a large part of the

water released from sediments, crust, and serpentinized mantle down to 410 km depth. Water concentration in those dense hydrous magnesium silicates is generally higher than 5 wt.% (Phase A, C, D, E) [5]. Moreover, partial melting of upward mantle plastic flow at the top the transition zone could induce a return flow of water down to the transition zone along subducted regions [8,12] and make portions of the slab well hydrated. In total, there is likely to be a significant slab flux of water into the top of the transition zone. The double diffusive mechanism described here can, in turn, extract this water into the transition zone. We therefore examine how much of the injected slab water flux is absorbed into the transition zone by this double diffusion mechanism.

3.2.1. Effects of thermo-chemical coupling on water flux

The flux of water away from the slab is given by Eq. (5) and can be inferred from Fig. 4 which displays the water concentration profile as a function of η for E ranging from 100 to -100 kJ mol^{-1}. At the interface between the slab and the mantle the concentration is approximately linear in η such that $C = \beta - \gamma\eta = \beta - \gamma\frac{z}{2\sqrt{\kappa t}}$, where γ and β are two arbitrary constants that will be estimated from the fit of the concentration profile. In a constant solubility case, the water flux can thus be approximated as:

$$\mathbf{J}_W^C \big|_{z=0} = -\alpha \frac{\partial C}{\partial z} = \alpha \frac{\gamma}{2\sqrt{\kappa t}} \tag{13}$$

If the solubility is temperature-dependent, using a Taylor expansion around zero of Eq. (6) and noting
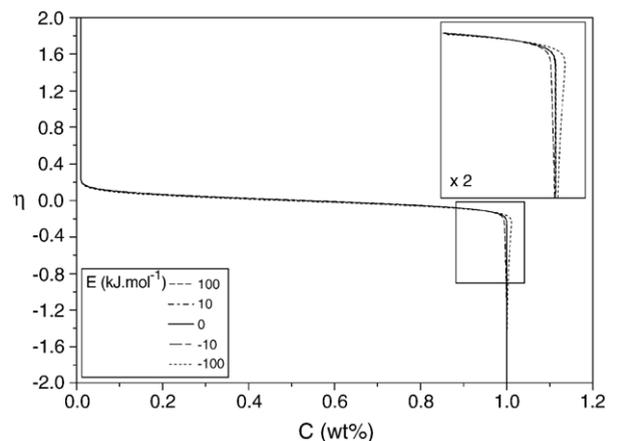
Fig. 4. Water concentration profile for several values of E. Water concentration profile of a 1%-wet slab diffusing in a dry surrounding mantle (0.1 wt.%) for a range of intrinsic chemical potential E. A water diffusivity α of $10^{-8} \text{ m}^2 \text{ s}^{-1}$ is used (one order of magnitude smaller than is Fig. 2). Axes are the same than in Fig. 2.

that when η is small, $\theta = \mathrm{erf}(\eta) = \eta$, we see that $\frac{C}{\bar{C}*} = \frac{\beta' - \gamma' \eta}{1 + A\eta}$ is approximately (Taylor expansion around zero) $\frac{C}{\bar{C}*} \sim \beta' - (\gamma' + \beta' A)\eta = \beta' - (\gamma' + \beta' A)\frac{z}{2\sqrt{\kappa t}}$, where γ' and β' are two arbitrary constants similar to γ, β. The total water flux is therefore given by:

$$\mathbf{J}_W|_{z=0} = -\alpha \bar{C}* \frac{\partial}{\partial z}\frac{C}{\bar{C}*} = \alpha \bar{C}* \frac{\gamma' + \beta' A}{2\sqrt{\kappa t}} = \alpha \frac{\gamma^*}{2\sqrt{\kappa t}} \quad (14)$$

Because the intrinsic solubility $\bar{C}* = e^{A\theta} = e^{A\,\mathrm{erf}(\eta)} = 1$ at the edge of the slab ($\eta = z = 0$), $\gamma^* = \gamma' + \beta' A$.

A useful variable to look at is the normalized water flux $\frac{\mathbf{J}_W}{\mathbf{J}_W^C}$. Using Eq. (5) at the slab-mantle interface we have:

$$\frac{\mathbf{J}_W}{\mathbf{J}_W^C}\bigg|_{z=0} = 1 + \frac{\mathbf{J}_W^*}{\mathbf{J}_W^C}\bigg|_{z=0} = \frac{\gamma^*}{\gamma} \quad (15)$$

In the numerical experiment displayed in Fig. 4, $A = \frac{E}{R\bar{T}}\frac{\delta T}{2\bar{T}}$ is known and the parameters γ, γ^* can be evaluated. For this case the normalized water flux goes from 1.09 to 0.91 for $E \in [100, -100]$ (kJ mol^{-1}). As expected, when the solubility increases with temperature ($E > 0$) the flux of water away from the slab is higher than in the constant temperature case and conversely when the solubility decreases with temperature ($E < 0$).

To estimate the effect of the coupling between heat and chemical diffusion on the flux, let us define an arbitrary reference by estimating the normalized flux assuming that the two diffusive processes are independent and uncoupled (uc). In this case (see Appendix B.3 for details), the two water fluxes at $z = \eta = 0$ are:

$$\mathbf{J}_W^C|_{z=0}^{uc} = -\alpha \frac{\delta C}{2\sqrt{\pi}\sqrt{\kappa t}} \quad (16)$$

and

$$\mathbf{J}_W^*|_{z=0}^{uc} = -\alpha \frac{\bar{C}}{2\sqrt{\pi}\sqrt{\kappa t}}\frac{E\delta T}{R\bar{T}^2} \quad (17)$$

Thus the 'uncoupled' normalized flux is:

$$\frac{\mathbf{J}_W}{\mathbf{J}_W^C}\bigg|_{z=0}^{uc} = 1 + \frac{E\delta T}{R\bar{T}^2}\frac{\bar{C}}{\delta C} \quad (18)$$

Now we can compare this 'uncoupled' normalized flux with the 'actual' normalized flux given by our model. The study of the two normalized water fluxes for $E = -100$ kJ mol^{-1} displayed for a range of δC in Fig. 5 yields two conclusions.
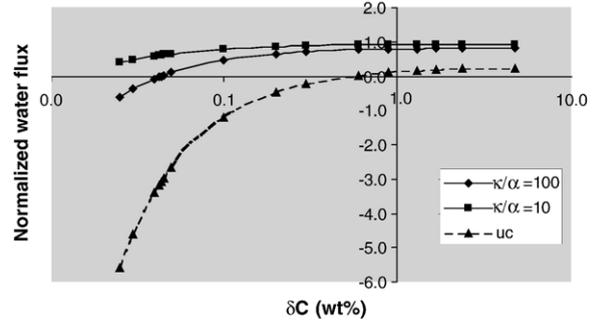
Fig. 5. Effect of the initial concentration step δC on water flux away from the slab Normalized water fluxes (total water flux over pure chemical water flux ratio) as function of the initial water concentration step between slab and mantle(δC (wt.%)) for two water diffusivities ($\alpha = 10^{-8}$, 10^{-7} m^2 s^{-1}) compared to the normalized flux if the heat and water diffusion processes were uncoupled (dashed line, see Appendix B.3). The normalized water flux is almost constant and close to one for high slab concentration ($\delta C > 0.5$ wt.%) and decreases rapidly for lower values. This plot demonstrates that the coupling strongly mitigates the decrease of water flux induced by the high solubility of the cold slab (see details in the text). The thermal diffusivity is set to be 10^{-6} m^2 s^{-1}. The mantle water concentration is fixed to 0.1 wt.% and $E = -100$ kJ. mol^{-1}.

First, 'actual' normalized flux follows a relation such as $\frac{\mathbf{J}_W}{\mathbf{J}_W^C}|_{z=0} = 1 - f\frac{1}{\delta C}$ where f is a constant. This $\frac{1}{\delta C}$-dependence is similar to the 'uncoupled' flux dependence (cf. Eq. (18)). Nevertheless, in this case, f is a function of $\frac{\kappa}{\alpha}$ in addition to the other variables (E, $\bar{C}$, δT, $\bar{T}$). In both cases, for a well hydrated slab (large initial concentration step between the slab and the mantle, i.e. $\delta C > 0.5$ wt.%), the water flux is weakly δC-dependent. When δC is smaller, the temperature driven flux is more important and its effects on the water flux becomes stronger. The total water flux away from the slab is lower and eventually, when δC is small enough, the temperature driven flux prevails, the total flux becomes negative and the water diffuses towards the slab.

Secondly, the coupled normalized flux is clearly higher than the 'uncoupled' normalized flux, by a factor of four for large δC and by more than a factor of ten for small δC (as said above the coupling can even change the sign of the flux for very small δC). The coupling of chemical and heat transport diminishes the influence of variable intrinsic solubility on the flux of water from the slab. By forming local maxima in concentration which increase the concentration gradients, the coupling mitigates the reduction in water flux (see Section 3.1.1). This self-regulation effect controls the strength of the chemically driven flux; it is constant for high initial water concentration δC and becomes stronger for low δC. As an example, for $E = 100$ kJ mol^{-1} with mantle-like parameters ($C_{\mathrm{mantle}}^0 = 0.1$ wt.%, $\bar{T} = 1300$ °C,

$\delta T = 300$ °C), the threshold at which self-regulation becomes significant takes place around $\delta C = 0.5$ wt.% and seems independent of $\frac{\kappa}{\alpha}$.

3.2.2. Net water extraction

Let us consider a slab entering the transition zone, which initially (at $t=0$) holds C_{slab}^0 in wt.% of water in a d-thick layer. The amount of water extracted from this slab lingering in the transition zone can be calculated using our model formulation. The amount of water in a vertical slice of this slab is $C_{slab}^0 d$. We integrate $\mathbf{J}_W$ in time over the area of the slab in the transition zone, to obtain the mass of water removed from this slice of slab during its transit across the transition zone. The mass of water removed is thus:

$$
\begin{aligned}
M_{H2O}^{rem} &= \rho \int_S \int_0^{t_{trans}} \mathbf{J}_W|_{z=0} \mathrm{d}t \mathrm{d}S \\
&= \left[\frac{\alpha \gamma^*}{\sqrt{\kappa}} \sqrt{t} \right]_o^{t_{trans}} S\rho
\end{aligned}
\tag{19}
$$

where S is the top surface area of the slab slice lying horizontally in the transition zone, t_{trans} the transit time and ρ is bulk mantle density. We can look at the ratio between the incoming and the removed mass of water in the slab for the two extreme cases when $E=-100$ kJ mol^{-1} and $+100$ kJ mol^{-1}.

$$
R\pm = \frac{M_{H2O}^{rem}}{M_{H2O}^{incoming}} = \frac{\frac{\gamma_+^* \alpha}{\sqrt{\kappa}} \sqrt{t_{trans}}}{C_{slab}^0 d}
\tag{20}
$$

where $\gamma_{\pm}^*$ corresponds to $E=\pm 100$ kJ mol^{-1}.

Consider the first case displayed in Fig. 4 as an example where the initial concentrations are $C_{slab}^0 = 1$ wt.% and $C_{mantle}^0 = 0.01$ wt.%. Measuring the slope of the curves at the slab-mantle interface, we obtain values for $\gamma_{\pm}^*$. For $E=100$ (kJ mol^{-1}), $\gamma_+^* = 6.08$ and for $E=-100$ (kJ mol^{-1}), $\gamma_-^* = 5.10$. According to tomographic imaging [7], we can assume a typical transit time of $t_{trans} = 50$ My. Considering that the hydrated region of the slab is about $d=5$ km thick and the water diffusivity $\alpha = 10^{-8}$ m^2 s^{-1}, the percentages of initial water removed from the slab are $R_+ \sim 48$% and $R_- \sim 40.5$% (or, respectively 68% and 57% for 100 My transit time).

The water flux is obviously diffusivity dependent (see Fig. 5). However, the water diffusivity of transition zone minerals is still not well constrained, firstly due to its temperature and pressure dependence, and secondly because grain boundary diffusion is likely to be orders of magnitude more effective than volumetric diffusion. The possible range for volumetric diffusivity α is from 10^{-10} m^2 s^{-1} [20] to 10^{-7} m^2 s^{-1} [21] which yields
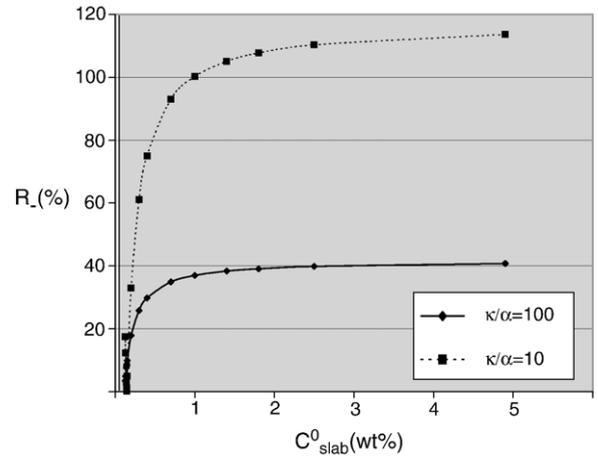
Fig. 6. Effect of the initial slab water concentration C_{slab}^0 on the mass of water removed from the slab. R_- the ratio between the incoming and the removed mass after 50 My for $E = \mu^0 - \frac{L_{21}}{L_{22}} = -100 kJ \, mol^{-1}$, as function of the initial slab water concentration C_{slab}^0 (wt.%) for two water diffusivities ($\alpha = 10^{-8}$, 10^{-7} m^2 .s^{-1}). Higher water diffusivity leads to larger amounts of water removed to the transition zone. R_- decreases significantly as the initial concentration C_{slab}^0 falls below 0.5 wt.%. The thermal diffusivity is set to be 10^{-6} m^2 .s^{-1} and the mantle water concentration is fixed to 0.1 wt.%.

another degree of freedom to the system in that $\frac{\kappa}{\alpha}$ varies from 100 to 10,000. Considering a higher water diffusivity, $\alpha = 10^{-7}$ m^2 s^{-1}, that could be relevant if grain boundary diffusion is efficient at this depth, leads to high R values: $R_+ \sim 174$% and $R_- \sim 107$%. In this case, the slab is totally dry after 50 My, regardless of the value or sign of E (see Fig. 6). For $\alpha = 10^{-9}$ m^2 s^{-1}, R decreases to around 15%.

For higher C_{mantle}^0, the values of $R\pm$ are lower. For example (see Fig. 6), with $C_{mantle}^0 = 0.1$ wt.% and $C_{slab}^0 = 1$ wt.%, we obtain $R_- \sim 36$%. For less hydrated slabs (i.e. with smaller C_{slab}^0 and δC), the flux and $R\pm$ start to decrease for slabs with concentration $C_{slab}^0 < 0.5$ wt.%.

4. Conclusion and discussion

We have analyzed the hydration of the Earth's mantle transition zone by diffusion of water out of slabs cooling within the transition zone. During this process, the coupling of water transport to thermal diffusion through temperature-dependent water solubility has two main consequences. First, if the intrinsic solubility of water is decreasing with increasing temperature ($E<0$), the coupling mitigates the effect of solubility variability on diffusive flux, thus the water flux estimation through simple (genuinely chemically driven) diffusion law can be seen as relatively robust. Indeed, when the water flux diminishes because of the low solubility in the warm

mantle, the system self-adjusts through the formation of a local concentration maxima below the edge of the slab, which in return increases the flux of water out of the slab. High water diffusivity and a low initial hydration of the slab both allow the thermal diffusion effect to be more efficient to keep water within the slab. If the standard-state chemical potential E of water in the mineral is strongly negative and the slab is close to saturation, the coupling mechanism can allow the water concentration to reach the saturation limit and thus induce fluid exsolution or melting. In particular, the formation of a peak water concentration at the edge of the slab can result in a super saturated area, where minerals will have to dehydrate and thus the formation of a fluid is likely. The partitioning of incompatible elements into this fluid implies that part of the slab could be depleted as it enters the lower mantle. Additionally, in case the solubility limit is reached, the presence of fluid (or melt) could enhance the water flux away from the slab because water preferentially partitions into aqueous solution or melt.

The main limitation of our model concerns the slab side boundary condition, since we assume that the concentration in the slab is fixed at infinity to allow similarity solution; thus we don't take into account water diffusion from the edge of the slab to its center. This assumption is correct for the early stage of the slab's traverse across the transition zone, when the thermal and chemical boundary layer are thin, but its validity diminishes with time. This potentially reduces the flux of water away from the slab. However, when the slab enters the transition zone, it has already undergone some chemical equilibration which would broaden the thickness of the slab's hydrated layer, which is consistent with our assumption of a uniform water concentration deep in the slab.

To infer quantitative predictions from our model, several parameters need to be constrained. The first is the temperature dependence of the solubility. At low temperature $<1200\ °C$, only pure water is present in the reaction and its fugacity is known. Assuming that the Soret effect is weak, E can be evaluated. In wadlseyite, known solubility is increasing with increasing temperature and $E \approx 20$ kJ mol^{-1} (cf. Appendix C). On the contrary at higher temperature Demouchy et al. [14] noted the presence of the fluid phase in measurements of wadsleyite water storage capacity at high P–T conditions, which influences interpretation of water solubility (mainly because the fugacity of the liquid phase is unknown). The thermal state of the slab also needs to be constrained. In addition to affecting the solubility temperature-dependence, the slab temperature field

(like the pressure field) controls the initial water concentration of the slab (when it enters into the transition zone). However, the geotherm of a slab at transition-zone depths is still under discussion. A cold slab [22] is likely to carry a lot of water down to the transition zone and the temperature difference with the surrounding mantle is high ($\sim 1000\ °C$) thus the solubility difference would be large and the effect of peak concentration could be considerable. In a warmer slab [23], these effects would be less efficient but in the meantime a younger, warmer, slab is likely to float much longer in the transition zone than will an old slab [24] and this will increase the time-integrated slab dehydration. Our model points out the importance of considering solubility variation with temperature in the study of water circulation in the mantle and should provide impetus for laboratory experiments to explore water solubility and transport properties in the deeper mantle.

Appendix A. Basic thermodynamics of water solubility

Chemical potential is the main controlling parameter of the diffusion process [17]. For water dissolved in solid, the general chemical potential is given by:

$$\mu = \mu^0 + RT\ln(a) = \mu^0 + RT\ln(C) \qquad (A.1)$$

where, the activity a equals the concentration C and μ^0 is the standard-state chemical potential of the substance in the state it assumes when dissolved (namely H^+).

The chemical reaction between water and the mantle transition-zone phases is commonly described, in Kröger–Vink notation [25] (where in superscripts indicate the charge with respect to an ideal crystal such that X is neutral, ● is positive and ′ is negative; alphabetic subscripts represent the crystallographic site), as :

$$H_2O + Mg_{Mg}^{X} \rightleftharpoons (2H)_{Mg}^{x} + MgO_{srg} \qquad (A.2)$$

where the hydroxyl incorporation is charge-balanced by Mg vacancies (V_{Mg}), a Mg atom being replaced by two H (or more rigorously by $[2OH_o^{\cdot} - V_{Mg}'']^X$), the magnesium atom (Mg) will form oxide and go to sites of repeatable growth (srg) such as grain boundaries [6].

When the minerals are in equilibrium with free fluid, the water concentration is the solubility C^* and we can write the equality of chemical potentials for the hydration reaction:

$$\mu_{H_2O} + \mu_{Mg} = \mu + \mu_{MgO} \qquad (A.3)$$

Or using $\mu_X = \mu_X^0 + RT \ln a_X$,

$$\mu_{H_2O}^0 + RT \ln\left(\frac{f_{H_2O}}{P_0}\right) + \mu_{Mg}^0$$
$$= \mu^0 + RT \ln(C^*) + \mu_{MgO}^0 + RT \ln(a_{MgO}) \qquad (A.4)$$

We can eliminate μ^0 between Eqs. (A.4) and (A.1), to obtain the final expression for chemical potential of dissolved water in terms of solubility limit C^* (4) used in the Section 2.1.

Appendix B. Fluxes and water diffusion

B.1. Phenomenological coefficients estimate

Following De Groot and Mazur [17], we can write an explicit form of the entropy balance equation, which in our case only includes thermal and chemical fluxes:

$$\rho \frac{ds}{dt} = -\nabla \cdot \left(\frac{\mathbf{J}_T - \mu \mathbf{J}_W}{T}\right) - \frac{\mathbf{J}_T}{T^2} \cdot \nabla T - \mathbf{J}_W \cdot \nabla \frac{\mu}{T} \qquad (B.1)$$

where ρ is the total density, s is total specific entropy, T is the temperature, μ the chemical potential of water and $\mathbf{J}_T$ and $\mathbf{J}_W$ are respectively the heat and chemical (water) flux. It follows that the expressions for the entropy flux and the entropy production rate are given by:

$$J_s = \frac{1}{T}(J_T - \mu J_W) \qquad (B.2)$$

$$\sigma = -\frac{1}{T^2} \mathbf{J}_T \cdot \nabla T - \mathbf{J}_W \cdot \nabla \frac{\mu}{T} \qquad (B.3)$$

By inspecting the local entropy production rate σ, one can define the fluxes and conjugate forces describing our system. According to the second law of thermodynamics, the rate of entropy production is positive definite, thus the heat flux $\mathbf{J}_T$ and the chemical (water) flux $\mathbf{J}_W$ are coupled by the positive definite matrix presented in Eq. (1).

It is useful to note that by introducing a new flux $\mathbf{J}_T' = \mathbf{J}_T - h_W \mathbf{J}_W$ (where h_W is the specific partial enthalpy of the water) (B.3) can be also written as:

$$\sigma = -\frac{1}{T^2} \mathbf{J}_T' \cdot \nabla T - \frac{1}{T} \mathbf{J}_W \cdot [\nabla \mu]_T \qquad (B.4)$$

where the $[\nabla \mu]_T$ is taken at constant temperature. Thus, the fluxes and forces can be related by another, physically equivalent, positive definite matrix:

$$\begin{cases} \mathbf{J}_T' = L_{11}' \nabla T - L_{12}' [\nabla \mu]_T \\ \mathbf{J}_W = L_{21}' \nabla T - L_{22}' [\nabla \mu]_T \end{cases} \qquad (B.5)$$

where the off-diagonal coefficients L_{12}', L_{21}' are respectively referred to as the Dufour and Soret coefficients.

To estimate the value of the diagonal coefficients L_{11} and L_{22} in Eq. (1), let us look at the heat flux at a fixed chemical potential $\mathbf{J}_T|_\mu$ and the chemical flux at a constant temperature $\mathbf{J}_W|_T$. The two fluxes become:

$$\mathbf{J}_T|_\mu = +L_{11} \nabla \frac{1}{T} = -k \nabla T = -\kappa \rho C \rho \nabla T \qquad (B.6)$$

$$\mathbf{J}_{W|T} = -\frac{L_{22}}{T} \nabla \mu = -\frac{L_{22}}{T} \nabla(\mu_0 + RT \ln C)$$
$$= -\frac{RL_{22}}{C} \nabla C = -\alpha \nabla C \qquad (B.7)$$

where we see that $L_{11} = \kappa \rho C_P T^2$ and that $L_{22} = \frac{\alpha C}{R}$. In our system, the heat diffusivity is $\kappa = 10^{-6}$ m^2.s^{-1}, the water diffusivity $\alpha = 10^{-8}$ m^2.s^{-1}, the temperature $T \sim 1300$, the water concentration $C = 0.1-1$ wt.% $= 1.9/$, $10^2 - 19/$, 10^2 mol . m^{-3} and the chemical potential $\mu = \pm 100$ kJ mol^{-1}. So, we have $L_{11} \sim 5.10^6$ (J. K. m^{-1} .s^{-1}) and $L_{22} \sim 1.9 \ 10^{-6}$ (mol^2. K. J^{-1}. m^{-1} .s^{-1}).

If we consider that the two parts of the chemical flux $\mathbf{J}_W$ defined in (1) are of the same order of magnitude, we see that $L_{21} \sim \mu L_{22} \sim 19 \ 10^{-2}$ (mol. K. m^{-1} .s^{-1}). The Onsager theorem tells us that $L_{12} = L_{21}$ [18]. Thus, we can compare the two terms of the total heat flux $\mathbf{J}_T$ (cf. Eq. (1)), and see that $L_{11} \sim 5.10^6 \gg \mu L_{12} \sim 1.9 \ 10^4$ (J. K. m^{-1} .s^{-1}). Consequently, we have neglected the off diagonal part of the heat flux.

B.2. Water solubility and diffusion

The water diffusive flux $\mathbf{J}_W$ can be recast in term of water solubility C^*. Using Eq. (4), $\mathbf{J}_W$ in Eq. (2) becomes:

$$\mathbf{J}_W = -\frac{L_{22}}{T} \nabla \left(\Delta \mu^0 + RT \ln\left(\frac{f_{H_2O}}{P_0 a_{MgO}} \frac{C}{C^*}\right)\right) \qquad (B.8)$$

or after some algebra:

$$\mathbf{J}_W = -RL_{22} \nabla \ln\left(\frac{f_{H_2O}}{P_0 a_{MgO}} \frac{C}{C^* e^{-\frac{\Delta \mu^0}{RT}}}\right) \qquad (B.9)$$

From Eq. (A.4), we can obtain an expression for the solubility C^* given in Eq. (3) and we define the intrinsic solubility $\bar{C}^*$ given in Eq. (6); introducing these into Eq. (B.9), the water diffusion equation $\frac{dC}{dt} = -\nabla(\mathbf{z} \cdot \mathbf{J}_W)$ can be written as (see Eq. (7)):

$$\frac{dC}{dt} = \alpha \nabla \left(\bar{C}^* \nabla \frac{C}{\bar{C}^*} \right) \qquad (B.10)$$

where $\alpha = \frac{RL_{22}}{C}$ is the water diffusivity, which is assumed to be constant.

B.3. Uncoupled fluxes

To evaluate the effect of the coupling between heat diffusion and water diffusion through water solubility, we compare it to a reference flux. This reference flux corresponds to the sum of the two water sub-fluxes ($\mathbf{J}_W^*$, $\mathbf{J}_W^C$) described in (5) in an uncoupled case. Using the definition of the concentration $C = \bar{C} + \frac{\delta C}{2} \Phi(\eta)$:

$$\mathbf{J}_W^C = -\alpha \nabla C = -\alpha \frac{\delta C}{2} \nabla \Phi^{uc} \qquad (B.11)$$

where Φ^{uc} is the solution of the uncoupled water diffusion equation

$$\frac{dC}{dt} = \alpha \nabla^2 C \qquad (B.12)$$

that is a simple error function $\Phi^{uc} = \mathrm{erf}\left(\frac{z}{2\sqrt{\alpha t}}\right) = \mathrm{erf}\left(\eta\sqrt{\frac{\kappa}{\alpha}}\right)$. Thus, we read:

$$\mathbf{J}_W^C = -\alpha \frac{\delta C}{2\sqrt{\kappa t}\sqrt{\pi}} e^{-\frac{\kappa}{\alpha}\eta^2} \cdot \mathbf{z} \qquad (B.13)$$

Similarly, with $T = \bar{T} + \frac{\delta T}{2}\theta(\eta)$ and using the solubility approximation, the flux due to solubility gradients is $\bar{C}^* = Be^{A\theta}$ (see Eq. (11))

$$\mathbf{J}_W^* = \alpha C \nabla \ln \bar{C}^* = \alpha \left(\bar{C} + \frac{\delta C}{2} \Phi^{uc} \right) \nabla A\theta \qquad (B.14)$$

where θ is the solution of the heat diffusion Eq. (8), a simple error function $\theta = \mathrm{erf}\left(\frac{z}{2\sqrt{\kappa t}}\right) = \mathrm{erf}(\eta)$ Eq. (9). Eq. (B.14) becomes:

$$\mathbf{J}_W^* = \frac{\alpha E \delta T}{R \bar{T}^2} \frac{e^{-\eta^2}}{2\sqrt{\kappa t}\sqrt{\pi}} \left(\bar{C} + \frac{\delta C}{2} \mathrm{erf}\left(\eta\sqrt{\frac{\kappa}{\alpha}} \right) \right) \cdot \mathbf{z} \qquad (B.15)$$

At the interface $z = \eta = 0$ and the fluxes are given by Eqs. (16) and (17) and the uncoupled normalized flux presented in Fig. 5 is given by Eq. (18).

Appendix C. Considerations on the term $E = \mu^0 - \frac{L_{21}}{L_{22}}$

One of the main parameters of the diffusion process is E the sum of μ^0 the standard-state chemical potential and $\frac{L_{21}}{L_{22}}$ which, in a sense, describes the importance of the thermal diffusion (Soret effect) compared to the chemical diffusion. Both of these terms are poorly constrained in transition zone minerals. A first order approximation of the standard-state chemical potential of water in wadsleyite could be drawn using recent experimental data and the solubility expression (3). Using only low temperature ($T < 1200$ °C) solubility data from Fig. 3(a) in Demouchy et al. 2005 [14] to avoid the solid–liquid partitioning effect, a linear fit gives an approximate value of $\mu^0 \approx 20$ kJ mol^{-1}.

The Soret effect is non-negligible in silicate liquids where it has been measured to be equal to a few dozens of kJ mol^{-1} [26], nevertheless to our knowledge, it has not been evaluated in solid-state diffusion at high pressure and temperature. Thus we have taken into account all the uncertainties considering a large range of possible values for these parameters $E \in [-100, +100]$ (kJ mol^{-1}).

Appendix D. Solubility and intrinsic solubility

The intrinsic solubility $\bar{C}^*$ is essentially controlled by the standard-state chemical potential μ^0, whereas the true solubility C^* includes the water fugacity. Consequently, even if these two variables are closely related, their temperature dependence can be opposite, depending on the water fugacity's temperature dependence. A first order fit of the water fugacity [15] by an exponential law $f_{H_2O} = Xe^{-\frac{Y}{RT}}$ gives $Y \simeq -140$ kJ mol^{-1}. Using it and $\Delta\mu^0 \simeq -351$ kJ mol^{-1} [27] in Eq. (6) shows that μ^0 could be as law as -211 kJ mol^{-1}, which still allows the true solubility to increase with increasing temperature as seen in the low temperature experiments [14] (i.e. $E + Y - \Delta\mu^0 > 0$). This demonstrates that the behavior of the solubility C^* and the intrinsic solubility $\bar{C}^*$ do not have to be the same.

References

[1] J. Dixon, L. Leist, C. Langmuir, J. Schilling, Recycled dehydrated lithosphere observed in plume-influenced mid-ocean-ridge basalt, Nature 420 (6914) (2002) 385–389.

[2] L. Ruepke, J. Phipps-Morgan, M. Hort, J. Connolly, Serpentine and the subduction zone water cycle, Earth Planet. Sci. Lett. 223 (2004) 17–34.

[3] T. Komabayashi, K. Hirose, K.-i. Funakoshi, N. Takafuji, Stability of phase A in antigorite (serpentine) composition determined by in situ X-ray pressure observations, Phys. Earth Planet. Inter. 151 (3–4) (2005) 276–289.

[4] M. Schmidt, S. Poli, Experimentally based water budgets for dehydrating slab and consequences for arc magma generation, Earth Planet. Sci. Lett. 163 (1998) 361–379.

[5] E. Ohtani, K. Litasov, T. Hosoya, T. Kubo, T. Kondo, Water transport into the deep mantle and formation of a hydrous transition zone, Phys. Earth Planet. Inter. 143–144 (2004) 255–269.

[6] D. Kohlstedt, H. Keppler, D. Rubie, Solubility of water in the alpha, beta and gamma phases of $(Mg, Fe)(2)SiO_4$, Contrib. Mineral. Petrol. 123 (4) (1996) 345–357.

[7] D. Zhao, Global tomographic images of mantle plumes and subducting slabs: insight into deep Earth dynamics, Phys. Earth Planet. Inter. 146 (1–2) (2004) 3–34.

[8] D. Bercovici, S. Karato, Whole-mantle convection and the transition-zone water filter, Nature 425 (2002) 39–43.

[9] X. Huang, Y. Xu, S.-I. Karato, Water content in the transition zone from electrical conductivity of wadsleyite and ringwoodite, Nature 434 (7034) (2005) 746–749.

[10] G. Richard, M. Monnereau, J. Ingrin, Is the transition zone an empty water reservoir? Inferences from numerical model of mantle dynamics, Earth Planet. Sci. Lett. 205 (2002) 37–51.

[11] G. Richard, M. Monnereau, M. Rabinowicz, Slab dehydration and fluid migration at the base of the upper mantle: implication for deep earthquake mechanisms, J. Geophys. Intl. (in press).

[12] G. Leahy, D. Bercovici, The dynamics of a heavy melt layer and water entrainment in the transition-zone water filter model, Earth Planet. Sci. Lett. (submitted for publication).

[13] T. Komabayashi, S. Omori, S. Maruyama, Petrogenetic grid in the system MgO–SiO2–H2O up to 30 GPa, 1600 C: Applications to hydrous peridotite subducting into the Earth's deep interior, J. Geophys. Res. 109 (B03206) (2004), doi:10.1029/2003JB002651.

[14] S. Demouchy, E. Deloule, D. Frost, H. Keppler, Pressure and temperature-dependence of water solubility in Fe-free wadsleyite, Am. Mineral. 90 (7) (2005) 1084–1091.

[15] K. Pitzer, S. Sterner, Equations of state valid continuously from zero to extreme pressures for H2O and CO2, J. Chem. Phys. 101 (1994) 3111–3116.

[16] E. Ohtani, H. Mizobata, H. Yurimoto, Stability of dense hydrous magnesium silicate phases in the systems Mg_2SiO_4–H_2O and $MgSiO_3$–H_2O at pressures up to 27 Gpa, Phys. Chem. Miner. 27 (2000) 533–544.

[17] S.R. De Groot, P. Mazur, Non-Equilibrium thermodynamics, Dover Publication, 1984, pp. 48–53.

[18] L. Onsager, Reciprocal relations in irreversible processes, Phys. Rev. 37 (1931) 405–426.

[19] B.J. Wood, A. Pawley, D. Frost, Water and carbon in the Earth's mantle, Philos. Trans. R. Soc. Lond., A 354 (1771) (1996) 1495–1511.

[20] R. Hae, E. Ohtani, T. Kubo, T. Koyama, H. Utada, Hydrogen diffusivity in wadsleyite and water distribution in the mantle transition zone, Earth Planet. Sci. Lett. 243 (2006) 141–148.

[21] J. Ingrin, H. Skogby, Hydrogen in nominally anhydrous upper-mantle minerals: concentration levels and implications, Eur. J. Mineral. 12 (2000) 543–570.

[22] T. Irifune, N. Kubo, M. Isshiki, Y. Yamasaki, Phase transformation in serpentine and transportation of water into lower mantle, Geophys. Res. Lett. 25 (2) (1998) 203–206.

[23] P. Van Keken, B. Kiefer, S. Peacock, High resolution models of subduction zones: implications for mineral dehydration reactions and the transport of water into the deep mantle, Geochem. Geophys. Geosyst. 3 (10) (2002), doi:10.1029/2001GC000256.

[24] U. Christensen, Influence of chemical buoyancy on the dynamics of slabs in transition zone, Geophys. J. Res. 102 (B10) (1997) 22,435–22,443.

[25] F. Kröger, H. Vink, Solid state physics 3, Academic Press, 1956.

[26] C. Lesher, D. Walker, Solution properties of silicate liquids from thermal diffusion experiments, Geochim. Cosmochim. Acta 50 (1986) 1397–1411.

[27] J. Brodholt, K. Refson, An ab initio study of hydrogen in forsterite and a possible mechanism for hydrolytic weakening, J. Geophys. Res. 105 (B8) (2000) 18,977–18,982.